JMEPEG (2007) 16:308–313
DOI: 10.1007/s11665-007-9057-8

1059-9495/$19.00

Forming-Limit Diagrams for Hot-Forming of AA5083 Aluminum Sheet: Continuously Cast Material

Mary-Anne Kulas, Paul E. Krajewski, John R. Bradley, and Eric M. Taleff

(Submitted December 20, 2006; in revised form February 15, 2007)

Fine-grained AA5083 aluminum sheet is used for hot-forming automotive body panels with gas pressure in the superplastic forming (SPF) and quick plastic forming (QPF) processes. Deformation under QPF conditions is controlled by two fundamental creep mechanisms, grain-boundary-sliding (GBS) and solute-drag (SD) creep. The failure mechanisms of AA5083 materials under QPF conditions depend strongly on these deformation mechanisms and on the applied stress state. Failure can be controlled by flow localization, cavitation development or a combination of both. There is interest in using continuously cast (CC) AA5083 materials instead of direct-chill cast (DC) materials in QPF operations as a means of reducing material cost. However, CC and DC AA5083 materials can produce significantly different ductilities under hot forming. Rupture-based forming-limit diagrams (FLDs) have been constructed for a CC AA5083 sheet material under hot-forming conditions. Forming limits are shown to be related to the controlling deformation mechanisms. Differences between FLDs from DC and CC AA5083 materials are investigated. The differences in FLDs between these materials are related to differences in cavitation development.

Keywords automotive, aluminum, mechanical testing

1. Introduction

Quick plastic forming (QPF) is a mass-production manufacturing process used to produce complex automotive closure panels in fine-grained AA5083 aluminum sheet (Ref 1). The QPF process utilizes gas pressure and moving hot dies to form aluminum sheet in a manner similar to superplastic forming (SPF) processes. Because QPF operates at lower temperatures and faster strain rates than the traditional SPF processes, it can be used to produce parts at remarkably faster rates. Typical QPF operations are conducted at a temperature of 450 °C and at strain rates on the order of 10^{-2} s^{-1}. Large tensile ductilities are possible under QPF conditions because of the two creep deformation mechanisms which dominate flow in fine-grained AA5083 materials under these conditions, grain-boundary-sliding (GBS) and solute-drag (SD) creep (Ref 2). Both these mechanisms provide large tensile elongations through high strain-rate sensitivities. The GBS mechanism, which dominates deformation under SPF, generally controls deformation at the lowest strain rates and highest temperatures. The SD mechanism, which occurs in AA5083 and other Al-Mg-based alloys because of high Mg alloy content (>3 wt.%), controls deformation at faster strain rates and lower temperatures, typically up to the point of power-law breakdown (Ref 2, 3). Although the GBS mechanism is commonly thought to produce greater tensile elongations than the SD mechanism does, recent investigations have shown exceptions to this relationship when cavitation development during hot deformation is pronounced (Ref 4, 5). Flow localization and cavitation are both important to sheet failure under QPF conditions. Because both these failure mechanisms depend upon stress state, stress state is also important to failure.

The forming-limit diagram (FLD) is a representation of forming data traditionally used to understand and predict the effects of stress state on failure strains for room-temperature stamping of sheet metals. There have been a number of efforts to use FLDs to establish forming limits of aluminum sheet materials at elevated temperatures, primarily related to SPF conditions (Ref 6-8). Data from sheet aluminum materials for FLD construction can be obtained under hot-forming conditions through tensile tests and a series of gas-pressure bulging experiments with specific die geometries (Ref 9). Recent investigations have illustrated the importance of considering both deformation mechanism and failure mechanism in FLD construction to establish forming limits of an AA5083 material under QPF conditions (Ref 5). The AA5083 material previously studied was produced by direct-chill (DC) casting. Because of interest in using continuously cast (CC) AA5083 materials for QPF operations to reduce material cost, it is of interest to compare the forming limits of DC and CC AA5083 materials under QPF conditions. For the present investigation, a CC AA5083 sheet material was mechanically tested in tension, in plane-strain bulging and in balanced biaxial bulging at temperatures and strain rates characteristic of QPF and SPF processes. The goal of this investigation is to better understand the relative forming limits of DC and CC AA5083 materials under these forming conditions.

This article was presented at Materials Science & Technology 2006, Innovations in Metal Forming symposium held October 15-19, 2006 Cincinnati, OH.

Mary-Anne Kulas, Alcan-Voreppe Research Center, 725 rue Aristide Bergès, BP 27, 38341 Voreppe Cedex, France; **Paul E. Krajewski** and **John R. Bradley,** General Motors R&D Center, 30500 Mound Rd, Warren, MI 48090; **Eric M. Taleff,** Department of Mechanical Engineering, The University of Texas at Austin, 1 University Station C2200, Austin, TX 78712. Contact e-mail: taleff@mail.utexas.edu.

Table 1 Compositions of the AA5083 materials studied are given in wt.%

Alloy	Casting Method	Thickness	Mg	Mn	Fe	Si	Cu	Cr	Zn	Ti	Al
DC1	DC	1.2 mm	4.5	0.76	0.20	0.15	0.03	0.07	0.02	0.01	bal.
CC1	CC	1.0 mm	4.7	0.72	0.22	0.07	0.02	···	···	···	bal.

2. Experimental Procedure

The CC material, designated in this study as material CC1, was hot rolled and then cold rolled to a thickness of 1 mm. The composition of material CC1 is listed in Table 1. Data from material CC1 are compared in this study to data from a DC material, designated material DC1, of thickness and composition also reported in Table 1 (Ref 5). The CC1 and DC1 materials are same as materials CC-A and DC-C in references (Ref 2, 4). Both materials were obtained in the H18 condition and were recrystallized during heating, prior to testing, to fine grain sizes of approximately 8.0 μm for the CC1 material and 6.5 μm for the DC1 material (Ref 2). The CC1 and DC1 materials contain very different distributions of intermetallic particles, as shown in Fig. 1, with CC1 containing smaller, more numerous particles. These differences in microstructure were previously linked to earlier cavitation under hot tensile deformation in the CC1 material (Ref 4). The CC1 sheet material was subjected to three types of mechanical tests: (1) uniaxial tensile tests, (2) plane-strain bulge tests and (3) balanced biaxial bulge tests. Mechanical tests were conducted at temperatures of 450 and 500 °C and at strain rates of 3×10^{-2} s^{-1} and 3×10^{-4} s^{-1}. Tensile tests were conducted using dog-bone-shaped coupons loaded into shoulder-loading grips; straining was conducted at constant true-strain rates. The tensile coupon gage length was taken perpendicular to the sheet rolling direction. Plane-strain bulge tests were conducted by constraining a sheet in a tool with a rounded rectangular opening of 254×51 mm into which the sheet was allowed to freely form under constant applied gas pressure. The long axis of each plane-strain bulge specimen was taken parallel to the sheet rolling direction. The rectangular die has a 5 mm entrance radius and walls tapered at 15° from vertical. Balanced biaxial bulge tests were conducted by constraining a sheet in a tool with a 100 mm diameter cylindrical opening and 5 mm entrance radius, into which the sheet was allowed to freely form under constant applied gas pressure. Gas pressure for each bulge forming experiment was selected in order to obtain the desired average strain rate at the bulge apex, based upon forming time and final strain; a number of calibration experiments were used to determine the correct forming pressure. Sheet specimens were electrolytically etched with 2.5 mm diameter circle grids prior to bulge testing, and the deformed circle grids were used to measure local strains after forming. Typical examples of failed bulge specimens are shown in Fig. 2. In all elevated-temperature tests, specimens were allowed to equilibrate at the test temperature for approximately 15 min prior to straining; this assured complete specimen recrystallization prior to

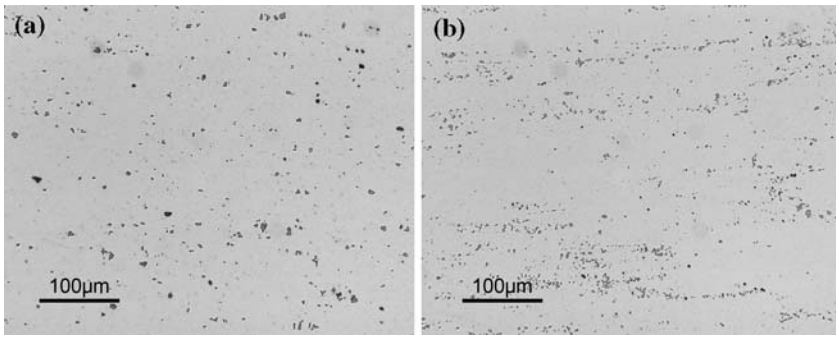

Fig. 1 As-received microstructures of the AA5083 materials (a) DC1 and (b) CC1 show the size and distribution of intermetallic particles

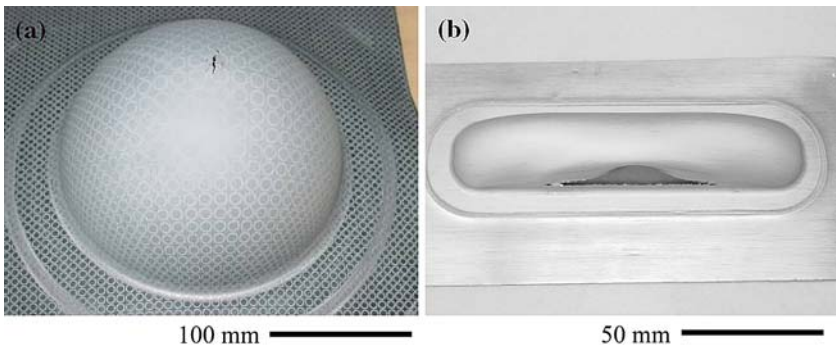

Fig. 2 Typical specimens failed during bulge testing under (a) biaxial stress and (b) plane strain conditions are shown

testing. Data for construction of FLDs were acquired by measuring local strains in ruptured and whole specimens tested in each of the three test types.

3. Results

FLDs were constructed as a major true strain against minor true strain for each test condition by plotting the strain combinations measured from whole specimens and those measured from ruptured specimens. Solid symbols represent combinations of major and minor strains reached without rupture, and open symbols represent strain states at which rupture was observed. FLDs containing data from conditions under which GBS dominates deformation (Ref 2), temperatures of (a) 450 and (b) 500 °C at a strain rate of 3×10^{-4} s^{-1}, are shown in Fig. 3. Tensile coupons ruptured by cavitation interlinkage with little or no flow localization, i.e. necking, when deformation was in the GBS creep regime (Ref 4). Specimens tested under plane-strain bulging failed with a length-wise rupture line close to the entrance radius, as is shown in Fig. 2(a). Specimens were oriented in the forming die with the rolling direction parallel to the long axis of the die. Thus, rupture is perpendicular to the rolling direction and produces a rupture line along the rolling direction, see Fig. 2(a). Because hot rupture is most likely to occur perpendicular to the sheet rolling direction, minimum major strain for rupture is measured in these experiments. Ruptures under plane strain were often catastrophic, complicating the measurement of strain

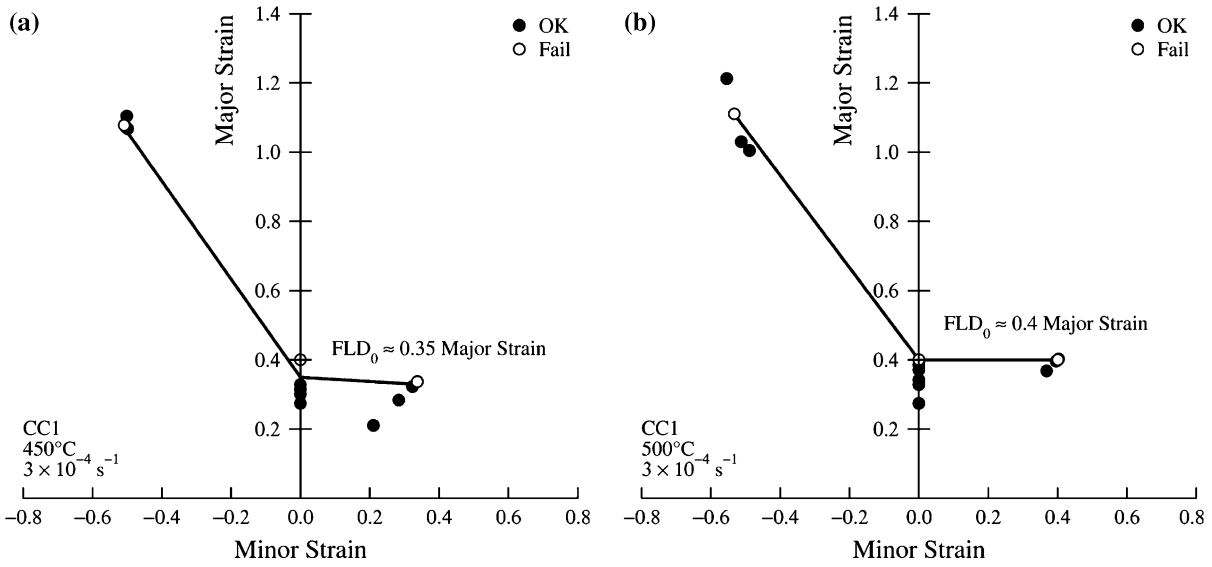

Fig. 3 Rupture-based forming limit diagrams are shown for AA5083 material CC1 at a strain rate of 0.0003/s and temperatures of (a) 450 °C and (b) 500 °C

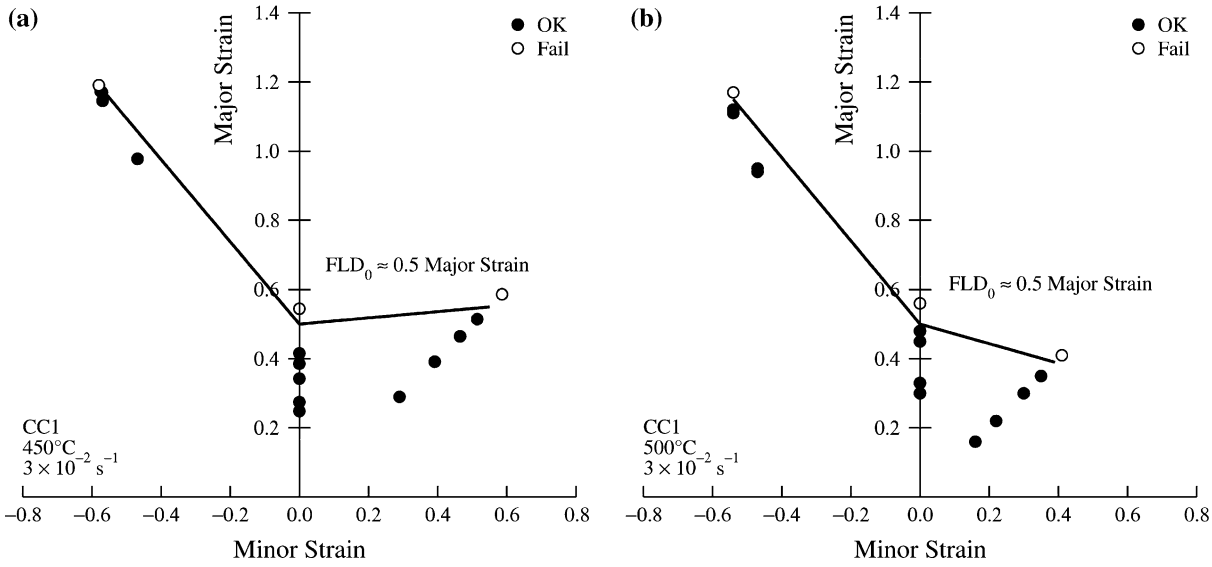

Fig. 4 Rupture-based forming limit diagrams are shown for AA5083 material CC1 at a strain rate of 0.03/s and a temperature of (a) 450 °C and (b) 500 °C

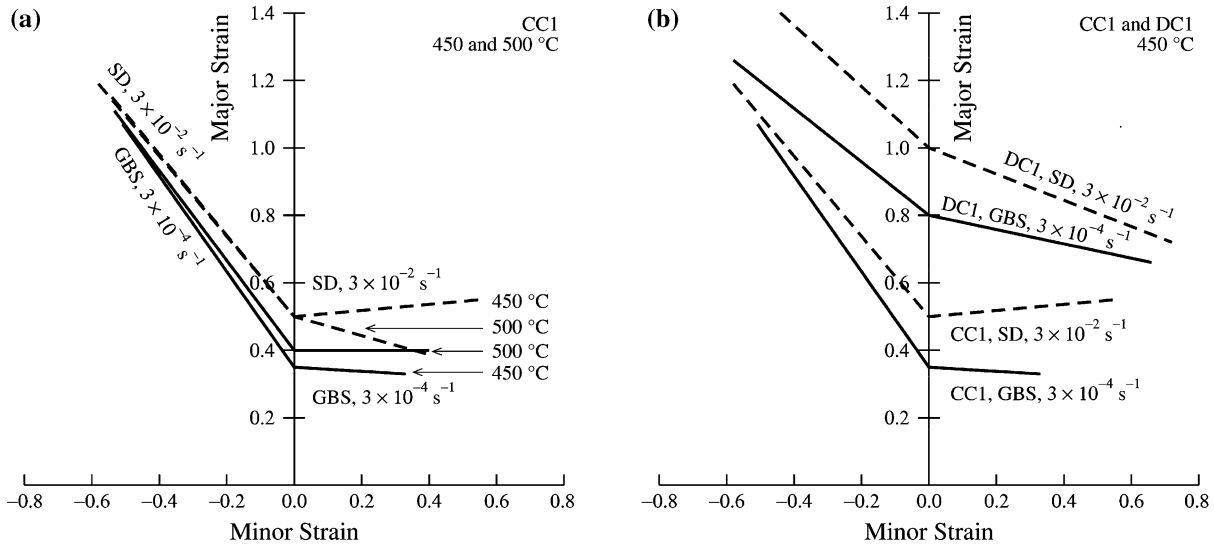

Fig. 5 Rupture-based forming limits are compared (a) between the various test conditions for the CC1 material and (b) between the CC1 and DC1 materials at 450 °C and two strain rates

and leading to uncertainty in the major strain at rupture under plane strain, i.e. FLD_0. Values reported for FLD_0 are estimates based upon the data shown. Rupture under balanced biaxial straining typically occurred near the dome peak, as shown in Fig. 2(b), and perpendicular to the rolling direction of the sheet. Lines representing forming limits shown on the FLDs were constructed using the approximate strains for failure under each of the three test geometries: (1) uniaxial, (2) plane strain and (3) balanced biaxial. An estimated value of FLD_0 is indicated in each FLD. FLDs containing data from conditions under which SD dominates deformation (Ref 2), temperatures of (a) 450 and (b) 500 °C at a strain rate of 3×10^{-2} s^{-1}, are shown in Fig. 4. Tensile coupons failed with strong flow localization preceding rupture by cavitation interlinkage when deformation was in the SD creep regime. The SD FLDs are similar in shape to the GBS FLDs, and approximate FLD_0 values are shown in each diagram.

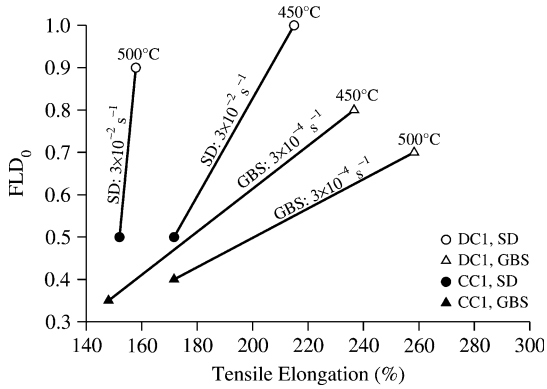

Fig. 6 Correlations are shown between FLD_0 and tensile elongation to failure at 450 °C and 500 °C. Data included are from both the DC1 and CC1 materials

4. Discussion

The FLDs produced for hot forming of AA5083 material CC1 sheet are unique to hot forming. The FLD_0 value is typically the minimum major strain along the forming limit for room-temperature FLDs. For hot forming of AA5083 sheet, however, the major strain on the forming limit in balanced biaxial tension can be minimum (Ref 5, 10). In the case of the CC1 material deformed under conditions for which GBS dominates flow, Fig. 3, the FLD_0 and the forming limit in balanced biaxial tension are approximately equal. Thus, the forming limit in the region of positive minor strain is nearly flat or of negative slope. As only three points were used in creating the forming limits shown in Fig. 3 and 4, no conclusion can be drawn for the curvatures of forming limits in the regions of positive and negative minor strain. Figure 5(a) shows the forming limits for all test conditions compared on a single diagram. This comparison clearly shows that the forming limits for deformation by SD creep are higher than those for GBS creep deformation. For a given deformation mechanism in Fig. 5(a), which corresponds to a given strain rate, a change in temperature from 450 to 500 °C only slightly alters the forming limit. However, a change in deformation mechanism from GBS to SD creep increases the forming limit strains under all stress states. This is opposite to the trend traditionally expected for superplastic materials, and differences in the cavitation evolution under SD and GBS creep is the cause of this effect. Cavitation volume fraction evolves much more rapidly with strain when deformation is by GBS creep than under SD creep (Ref 4). For material in which cavitation during hot forming is significant, as is the case for CC1, this difference is pronounced. Cavitation is also the cause of the unusual slope, approximately flat or negative, of the forming limit in the region of positive minor strain. Cavitation growth is typically fastest under balanced biaxial tension (Ref 10). When failure is controlled by cavitation, the major strain of the forming limit at balanced biaxial tension may be expected to be minimum or nearly minimum along the forming limit. This has also been shown to be the case for the DC1 material, forming limits of which are compared with those of the CC1 material in Fig. 5(b) at a temperature of 450 °C. The forming limit shapes of the

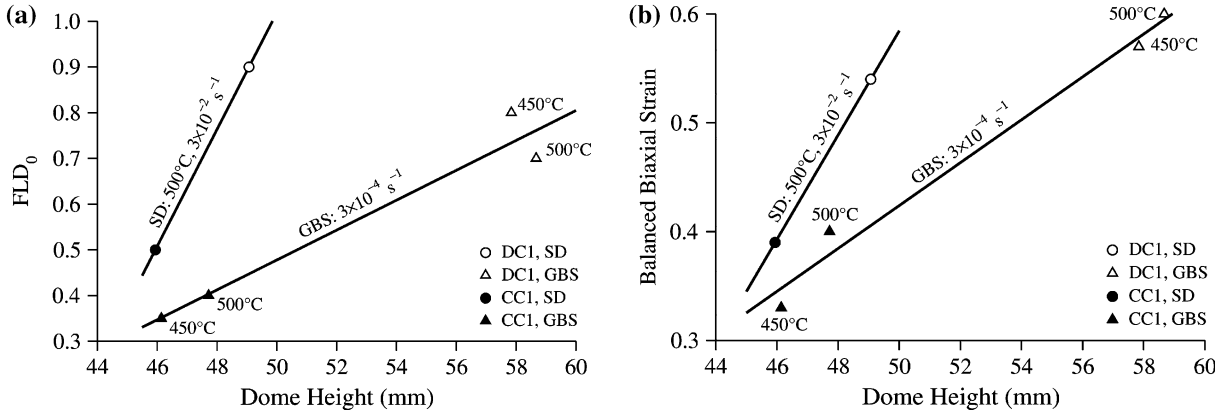

Fig. 7 Correlations are shown (a) between FLD_0 and dome height and (b) between balanced biaxial strain at failure and dome height at 450 and 500 °C. Data included are from both the DC1 and CC1 materials

DC1 material are similar to those of the CC1 material, but with a more negative slope in the region of positive minor strain. For the DC1 material, the forming limit under SD creep is again greater than that under GBS creep, and differences in cavitation development between deformation mechanisms is again the cause. The forming limits of the DC1 material are significantly higher than are those of the CC1 material. This is because the CC1 material develops significant cavitation at much smaller strains than does the DC1 material, which has been demonstrated for uniaxial tension in a previous study (Ref 4).

Because the construction of FLDs for hot forming requires specialized equipment and numerous tests, it is of interest to use a single forming test to characterize hot formability in industrial practice. Two types of experiments have commonly been applied to this end: (1) the uniaxial tension test and (2) balanced biaxial bulge forming. The correlations of these two types of experiments with FLD_0 are explored in Fig. 6 and 7. Figure 6 contains a plot of FLD_0 against percent tensile elongation, as measured in a simple tension test, for both materials CC1 and DC1. Data from these two materials at any given combination of temperature and strain rate show a clear correlation; FLD_0 increases with tensile elongation. The rate of increase in FLD_0 with tensile elongation increases remarkably as the deformation mechanism changes from GBS to SD creep. It is clear from these data that individual tension tests must be conducted at each potential combination of temperature and strain rate to predict FLD_0. Figure 7 (a) shows a plot of FLD_0 against maximum dome height achieved at failure under balanced biaxial stress in the bulge test geometry of the present investigation. These data show that FLD_0 correlates quite well with dome height for deformation controlled by a single deformation mechanism. Data from materials CC1 and DC1 at 450 and 500 °C under GBS creep clearly display a linear relationship between FLD_0 and dome height. Thus, balanced biaxial bulging experiments can be reasonably used within the GBS regime to predict FLD_0. The data taken under SD creep reveal a similar relationship, but with a steeper slope. Data for dome height under SD creep at 450 °C are not available because catastrophic rupture near the dome apex prevented accurate measurement of dome height. Because this results in only two data points for SD creep, the linear relationship assumed for SD creep in Fig. 7(a) must be considered speculative. The data obtained indicate that FLD_0 can be reasonably predicted by two balanced biaxial bulging experiments, one under each of the two pertinent deformation mechanisms. Balanced biaxial dome height has the added practical benefit of also being a good predictor of the forming limit under balanced biaxial straining, as might be expected. This is confirmed in Fig. 7(b), which contains a plot of balanced biaxial strain at failure against dome height at failure. Two linear relationships are revealed in the same manner as in Fig. 7(a), one for each of the two deformation mechanisms. Because the forming limit in balanced biaxial straining can be less than FLD_0, it is very important to know the forming limits under both of these stress states. Balanced biaxial bulging experiments can meet this requirement.

It should be noted that sheet thickness distributions after forming have not been evaluated in the present study, but are expected to differ between deformation under GBS and SD creep. Thickness distribution across the formed sheet constitutes yet another potential failure criterion, which merits additional investigation.

5. Conclusions

FLDs have been constructed for an AA5083 sheet material produced by continuous casting, material CC1. The forming limits of the CC1 material are lower than those of an equivalent AA5083 produced by direct-chill casting, material DC1. The lower forming limits of the CC1 material are associated with more severe cavitation during hot forming than in the DC cast material, which is consistent with previous investigations utilizing only tensile tests. The shapes of the FLDs for material CC1 are strongly influenced by cavitation during hot deformation, which results in forming a limit under balanced biaxial straining which is approximately equal to or less than the forming limit in plane strain, FLD_0. Forming limits for deformation under SD creep are higher than those for deformation under GBS creep; this effect was also observed for the DC1 material and is associated with more rapid cavitation evolution with strain under GBS creep. It is observed that dome height at failure from balanced biaxial bulging provides an excellent predictor of FLD_0 and balanced biaxial strain at failure for a given deformation mechanism. Thus, the industrial demand of a simple predictor for forming limits of a given AA5083 material under hot deformation can be

practically met by conducting two balanced biaxial bulging experiments, one under SD creep and a second under GBS creep.

References

1. J.G. Schroth, General Motors Quick Plastic Forming Process, in *Advances in Superplasticity and Superplastic Forming*, E.M. Taleff, P.A. Friedman, P.E. Krajewski, R.S. Mishra, and J.G. Schroth, Eds. TMS, Warrendale, PA, 2004, p 9–20
2. M.-A. Kulas, W.P. Green, E.M. Taleff, P.E. Krajewski, and T.R. McNelley, Deformation Mechanisms in Superplastic AA5083 Materials, *Metall. Mater. Trans. A*, 2005, **36A**, p 1249–1261
3. E.M. Taleff, An Overview of Creep Deformation Behaviors in 5000-Series and Al-Mg Alloys, in *Advances in Superplasticity and Superplastic Forming*, E.M. Taleff, P.A. Friedman, P.E. Krajewski, R.S. Mishra, and J.G. Schroth, Eds. TMS, Warrendale, PA, 2004, p 85–94
4. M.-A. Kulas, W.P. Green, E.M. Taleff, P.E. Krajewski, and T.R. McNelley, Failure Mechanisms in Superplastic AA5083 Materials, *Met. Metall. Mater. Trans. A*, 2006, **37A**, p 645–655
5. M.-A. Kulas, P.E. Krajewski, J.R. Bradley, and E.M. Taleff, Forming Limit Diagrams for AA5083 under SPF and QPF Conditions, *Materials Science Forum*, 2007, **551–552**, p 129–134
6. S.P. Keeler and W.A. Backofen, Plastic Instability and Fracture in Sheets Stretched over Rigid Punches, *Trans. ASM.*, 1963, **56**, p 25–47
7. S.P. Keeler, Rating the Formability of Sheet Metal. *Metal Progress*, 1966, **90**, p 148–153
8. G.M. Goodwin, "Application of Strain Analysis to Sheet Metal Forming Problems in the Press Shop," *SAE Transactions: SAE Paper No. 680093* (1968), p 380–387
9. J.R. Bradley, Bulge Testing of Superplastic AA5083 Aluminum Sheet, in *Advances in Superplasticity and Superplastic Forming*, E.M. Taleff, P.A. Friedman, P.E. Krajewski, R.S. Mishra, and J.G. Schroth, Eds. TMS, Warrendale, PA, 2004, p 109–118
10. D.H. Bae, A.K. Ghosh, and J.R. Bradley, Stress-State Dependence of Cavitation and Flow Behavior in Superplastic Aluminum Alloys, *Metall. Mater. Trans. A*, 2003, **34A**, p 2449–2463